A MULTI-PRONG STUDY ON AERODYNAMIC CHARACTERISTICS OF ARCHIMEDES SPIRAL-TYPE WIND TURBINE BLADE

Yoon Kee Kim[1], Qian Lu[1], Ho Seong Ji[1], Joon Ho Beak[2], Rinus Mieremet[3], Kyung Chun Kim[1,*]

[1] *School of Mechanical Engineering, Pusan National University, Jangjeon-dong, Geumjeong-Gu, Busan, Korea*
[2] *Department if Engineering Research, ESCO RTS, Doosanventuredigm, B112, Pyeongchon-Dong, 126-1, Dongan-Gu, Anyang, Gyeonggi-Do, Korea*
[3] *CTO and inventor, the Archimedes, Looiershof 30, 3024 CZ Rotterdam, the Netherlands*

**corresponding author: Tel.:+82-51-510-2324; fax: +82-51-515-7866*
E-mail address: kckim@pusan.ac.kr

Abstract

This research describes aerodynamic characteristics of small-scale wind turbine blade, called Archimedes spiral wind turbine blade. Numerical approaches on the prediction of aerodynamic performance of the blade have been conducted. Both steady and unsteady state numerical simulations using ANSYS CFX are performed on the several cases of rotating speeds. Large scale tip vortex is captured and graphically addressed in this research. In order to proving the results of numerical simulation, Particle Image Velocimetry (PIV) has been used to measure the aerodynamic characteristics of the Archimedes spiral wind turbine blade. Detail velocity vector fields around the blade are obtained and compared to those predicted by the steady and unsteady state CFD analysis. Mean velocity profiles are in a good agreement between experiment and unsteady state CFD analysis, the trajectory and magnitude of tip vortices generated by the blade are identified from the PIV results.

1. Introduction

In order to secure energy supply and cope with climate change, GHG (Green House Gas) emission reduction, biodiversity protection, renewable technologies development, energy conservation, and efficiency improvements have become the world's growing consensus. Among all renewable resources, wind energy has been proven to be a relatively matured technology and has tremendous potential in commercialization and mass production. Today the major application of wind power is electricity generation from large grid-connected wind farms [1]. With the expansion of power grid and the reduction of electricity scarce areas, small-scale wind turbine has now been applied in fields such as city road lighting, mobile communication base stations, offshore aquaculture and sea water desalination in several countries [2].

In this research, the special design originates from the Archimedes' screw [3]. Certainly, there is another thing inspires the design of the Archimedes spiral wind turbine: the Archimedes spiral, which known as the arithmetic spiral. The Archimedes spiral has the property that any ray from the origin intersects successive turnings of the spiral in points with a constant separation distance. The Archimedes spiral was used as a better way of determining the area of a circle. The spiral improved an ancient Greek method of calculating the area of a circle by measuring the circumference with limited tools. The spiral allowed better measurement of a circle's circumference and thus its area. However, this spiral was soon proved inadequate when Archimedes went on to determine a more accurate value of Pi that created an easier way of measuring the area of a circle [4].

In 2009, Timmer and Toet updated the Archimedes wind turbine model, which was built by the selective laser sinter method, and carried out a fundamental research to explore its potentials and find an optimum of its power output [5]. The highest efficiency measured in these circumstances was 12%. Effects created by an angle of 20 degrees or more, were positive to its efficiency. The measured air resistance coefficient laid around 1.3. Most likely this is the coefficient of the support system. Some air is pushed outward. Because of the air resistance of brake-engine, that was placed in the middle of the swept area. This pushed out air lowers the measured net efficiency. This should be examined later on. Shortening the model appears to have a positive effect on its efficiency.

There have been no tests performed with the actual size Archimedes wind turbine so far. Recently, Lu et al. [6] developed a design method of the Archimedes spiral wind turbine blade and performed a numerical simulation using ANSYS CFX v12.1. The radius of the 0.5kW class Archimedes wind turbine was 0.75m. The TSR-C_p diagram shows a typical parabolic relation in which the maximum efficiency of the blade approximately 25% exists at TSR=2.5.

In the present study, an experimental study is conducted to find out the aerodynamic characteristics and evolution of the tip vortex structures in the near wake of the Archimedes wind turbine model installed in an open type wind tunnel. The steady and unsteady CFD simulations on the Archimedes wind turbine are also conducted to test the capability as a design tool for the wind turbine. In addition, aerodynamic characteristics surrounding the wind turbine blade is investigated by using a PIV measurement system.

The focus of this research is on quantifying the evolution of the tip vortex properties and velocity distributions, including mean velocities and instantaneous velocities. This research will let us understanding the turbulent wake structures more deeply.

2. Numerical and experiment methods

2.1. Numerical method

2.1.1. Governing equation

Computational Fluid Dynamics (CFD) is a computer-based tool for simulating the behavior of systems involving fluid flow, heat transfer, and other related physical processes. It works by solving the equations of fluid flow (in a special form) over a region of interest, with specified conditions on the boundary of that region.

CFX, one of the analysis programs on fluid mechanics of CFD, which is idealized according to Reynolds Averaged Navier-Stokes Equation and the Finite Volume Method of Governing Equation. The SST (Shear Stress Transport) model has been used in order to predicting the separation of flow accurately [7]. So that, the Continuity Equation and Momentum Equation are shown as:

$$\frac{\partial \rho}{\partial t} + \nabla \cdot (\rho U) = 0 \tag{19}$$

$$\frac{\partial (\rho U)}{\partial t} + \nabla \cdot (\rho U \otimes U) - \nabla \cdot (\mu_{eff} - \nabla U) = -\nabla p + \nabla \cdot (\mu_{eff} - \nabla U)^T + B \tag{20}$$

Here, B is the total body force, μ_{eff} is the effective viscosity coefficient.

The Transport Equation of SST k-ω model can be shown as:

$$\frac{\partial}{\partial t}(\rho k) + \frac{\partial}{\partial x_i}(\rho k u_i) = \frac{\partial}{\partial x_j}\left(\Gamma_k \frac{\partial k}{\partial x_j}\right) + \tilde{G}_k - Y_k$$

$$\frac{\partial}{\partial t}(\rho \omega) + \frac{\partial}{\partial x_i}(\rho \omega u_i) = \frac{\partial}{\partial x_j}\left(\Gamma_\omega \frac{\partial \omega}{\partial x_j}\right) + G_\omega - Y_\omega \tag{21}$$

Here, $\tilde{G}_k$ is the generation of turbulent kinetic energy for the mean velocity gradient, and G_ω is shown as the generation of accumulation rate. For Γ_k, Γ_ω, Y_k, Y_ω, each of them is shown as the effective diffusivity and turbulence dissipation of k and ω.

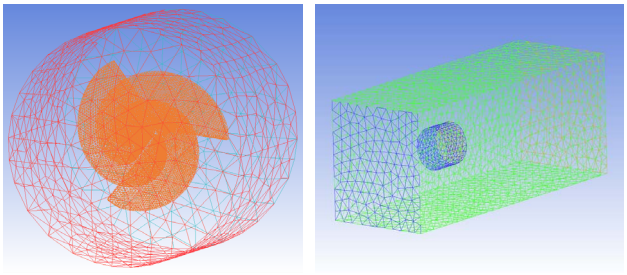

Fig. 1. Meshing of rotating and stationary domain

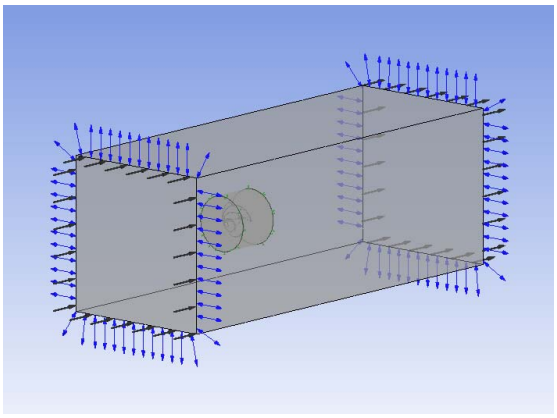

Fig. 2. Boundary condition setup on CFX-Pre

2.1.2. Mesh generation

All CFD problems are defined in terms of initial and boundary conditions. It is important that the user specifies these correctly and understands their role in the numerical algorithm. In transient problems the initial values of all the flow variables need to be specified at all solution points in the flow domain. Fig. 1 shows that a grid established at preparation phase including flow domain in order to computing the shape of blade on CFX. It separates the grid into the entire domain of using MFR (Multiple Frames of Reference) method, rotating domain of spiral blade and static domain of imaginary wind tunnel simulation. The grid number is about 292,935 on rotating domain, and about 50,106 on static domain, in total it consists of 343,041 grids.

2.1.3. Boundary condition

Grid make up by ICEM CFD and were established on CFD-Pre with analysis boundary condition is shown as Fig. 2. The size of imaginary wind tunnel is 0.4m x 0.4m x 1.5m, and let the boundary type is opening. In this simulation, we choose three cases to predict the aerodynamic characteristics with inlet wind velocity are 3.5m/s, 4m/s and 4.5m/s; rotating velocity are 300rpm, 400rpm and 500rpm, respectively. Three sharing surfaces of rotating and static domain applied the conservative interface flux for mass and momentum, and calculate the inlet and outlet air flow through boundary surface naturally. Using GGI (General Grid Interface) since the nodes inconformity on the boundary surface, and using physical value interpolation to adhere another node, the frame change model used frozen rotor.

2.2. Experiment method

PIV measurement was employed to acquire detailed flow information [8]. The experimental model of the Archimedes wind turbine blade is 1/10 scaled down model of 0.5kW wind turbine designed in our previous research [6],

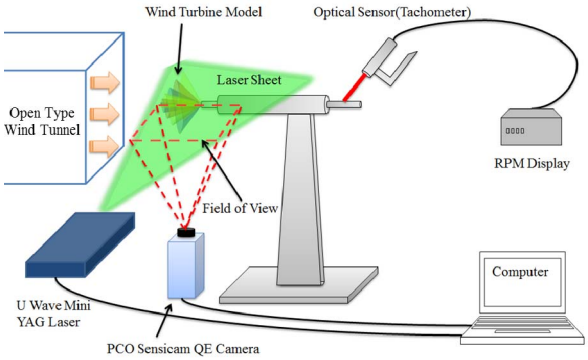

Fig. 3. Experimental setup for PIV measurement

so that the outer diameter of the model is 150 mm. The model was manufactured by a Rapid Prototyping method. As shown in Fig. 3, the Archimedes wind turbine blade was set behind the outlet of small-scale boundary layer wind tunnel; the blade was located at 100mm from the wind turbine exit. The attack wind profiles were measured at the tip of blade. And the outlet cross section of the wind tunnel is 300 mm by 300 mm, twice as the blade's diameter. That means there has enough space to investigate the evolution of aerodynamic characteristics and near wake structures. The PIV system was used to measure the velocity component in 2D plane from horizontal stream-wise (x-y plane). A U wave mini-YAG laser was used as the light source. The laser beam was transformed into a light sheet using cylindrical and spherical lenses. The field of view for velocity field measurement is about 150 mm by 120 mm corresponding to the CCD resolution of 1280 by 1024 pixels. A digital 12bit CCD camera (PCO Sensicam qe camera) fitted with 60mm lens was setup vertically under the Archimedes wind turbine to capture particle images in x-y planes. The mean velocity field was obtained by the conventional two frames cross correlation technique with 64 by 64 interrogation window size and 50% overlap. A total of 2000 instantaneous velocity fields were used to compute the ensemble averaged velocities, the turbulence intensities and Reynolds shear stresses. The vorticity can be calculated by the instantaneous velocity vectors, and by using a total of 2000 realizations instantaneous PIV measurements, the distribution of ensemble averaged vorticity field can be obtained [9].

3. Results and discussion

3.1. Results from CFD analysis

3.1.1. Steady state simulation

To investigate the results of aerodynamic characteristics, from left three figures of Fig. 4 to 6, it is shown that the computed ensemble average velocity fields of the overall flow field on the central of the Archimedes spiral wind

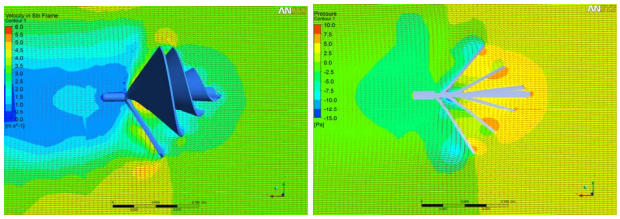

Fig. 4. Ensemble average velocity field and pressure distribution in steady state simulation (3.5m/s and 300rpm)

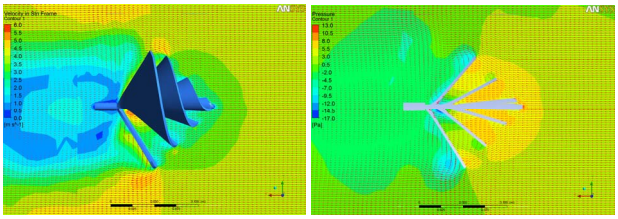

Fig. 5. Ensemble average velocity field and pressure distribution in steady state simulation (4m/s and 400rpm)

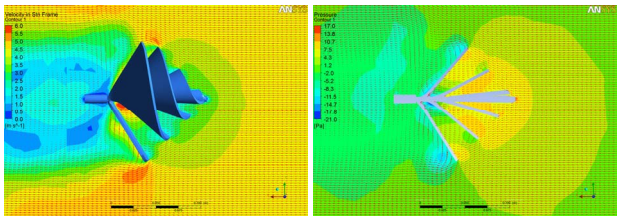

Fig. 6. Ensemble average velocity field and pressure distribution in steady state simulation (4.5m/s and 500rpm)

turbine at three different wind speeds, characterized by contours and vectors of velocity. Remarkably, that is the details of flow behavior that can be obtained at small wind velocities. Actually, the contours shown in these figures correspond to the turbulent wake state. For wind turbines effects occurs when the wind changes speed or direction, or when the rotor is subject to blade pitching actions. The highest velocities are seen at the inner outermost of the rotor in the domain. And because of the spiral effect, the velocities from the leading end become more and more quickly at the inner side of each level blades. There was a recirculation zone with lower speeds between each blade's spiral sectors. It can also be seen clearly that the incoming airflow was blocked by the hub cone and the rotor. A circular accelerating zone existed behind the rotor, which resulted in low pressure near the wall of rotating domain. Behind the hub of the rotor, a low-speed region was formed indicating the wake region. As expected, they show geometrically the airfoil with the more twisted angle at the root than the one at the tip. Graphically the longer arrows around the tip on the plots demonstrate that the incoming flow was faster at the tip than at the root. The three plots also suggest that the flow was much slower at the center than the edge. This suggests the stronger flow near the tips of blades would be very beneficial as the flow drives the blade with a longer moment arm.

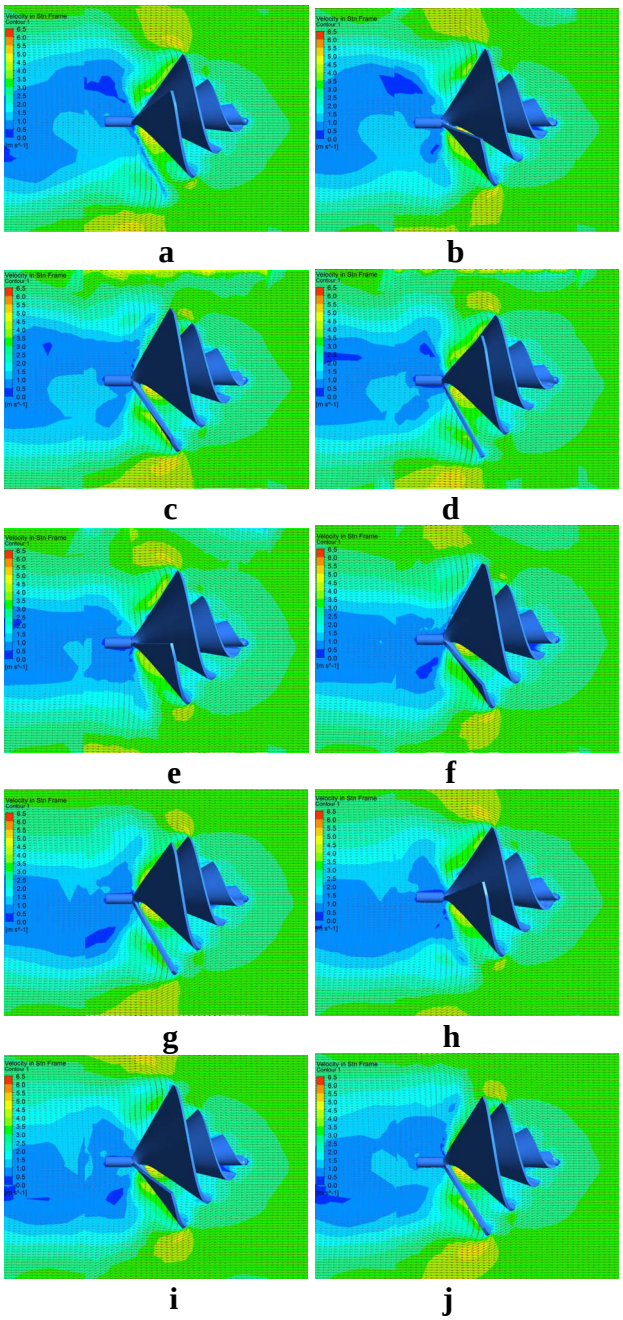

Fig. 7. Phase-locked ensemble average results in unsteady state simulation (3.5m/s and 300rpm)

Right three figures of Fig. 4 to 6 show that evenly distributed surface pressure on the pressure side of the rotor; these were achieved by twisting the blade gradually more towards the tip. The differences were just around 3 Pa between the root and the tip, but on the suction side, the differences were much bigger, the pressures were over 15 Pa (even over 20 Pa at 4,5m/s wind speed) lower at the tip than the root. Therefore the pressure difference between the two sides at a section increased towards the tip of each blade.

3.1.2. Unsteady state simulation

Fig. 7 shows the phase-locked ensemble averaged results for 3.5 m/s wind speed and a rotating speed of 300 rpm is representative of this case. A vertical visualization plane (X-Z plane) has been used through the core of the blade. And it is possible to see the variation in the strength of the tip vortex structures as the rotor blades find themselves at different phase angles from 0° to 360°, with interval of 36°. Fig. 7(a) illustrates the onset of the tip vortex structure on the leading edge separation with the boundary layer beginning to detach from the blade. Fig. 7(b) shows the enhance of the tip vortex structure, which in Fig. 7(c) the core area of the tip vortex becomes more and more clearly and moves downstream, at last the tip vortex has been get to peak and separate from the blade, which was shown in Fig. 7(d). Fig. 7(e) shows that a newly tip vortex structure is building up, and will repeat the phenomenon. From Fig. 7(f) to Fig. 7(j), there was another evolution of tip vortex structure appeared in the upper side of the blade, and moves upstream, similar with the downstream one. The phase-locked ensemble average results in 4 m/s and 4.5 m/s, and the rotating speed were 400 rpm and 500 rpm respectively are similar tendency with the results that shows in Fig. 7. In unsteady state, the maximum value of velocity can be seen at the inner outermost and the tip vortex core of the rotor in the domain, such as shown in the results of steady state cases.

3.2. PIV measurement results

The results of ensemble averaged PIV measurement of all instantaneous fields are shown on Fig. 8(a) to 8(c). Here, one can see the incoming air flow can be found to decelerate significantly when it flows across the wind turbine blades. And obviously, it can be seen that the incoming wind speed is much higher than that of local wind speed under blade's rejection. So that, it shows that the position of the kinetic energy of the airflow associated with the velocity deficits has been harvested by the wind turbine. The deformation of

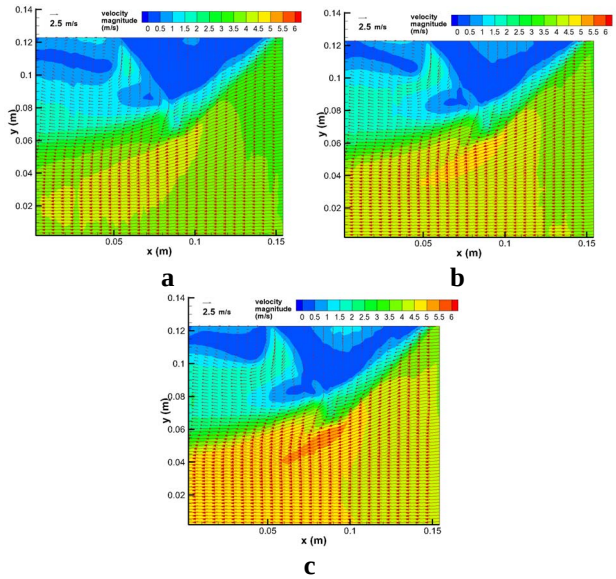

Fig. 8. Ensemble averaged velocity field near blade tip (**a**: 300rpm and U_∞ = 3.5m/s; **b**: 400rpm and U_∞ = 4m/s; **c:** 500rpm and U_∞ = 4.5m/s)

flow tube surface is clearly seen due to the tip vortices. It should be noted that there is a large scale vortex structure, which results from a separation behind the blade. The investigation of the time series of instantaneous velocity fields show that there is a fluctuation in the position of the cores of the tip vortices. These fluctuations produce a reduction of vortex intensity when the average values are calculated from the instantaneous fields. The analysis of near rotor wake shows that the blade is a major source of disturbances and unsteady aerodynamic effects. This is due to the spiral shape of the blade. The effects of the rotation speed and wind speed, which means the tip-speed-ratio, of the wind turbine model on the aerodynamic characteristics in the wake were also surveyed. The three PIV experiment results show that they have a similar wake flow mark, and at the same time those contours show that the only differences were just from the comparison of the plots at different tip-speed-ratios. It is obvious that the velocity reductions in the wake region with relatively low tip-speed-ratio are found to be much smaller than that the case with relatively high tip-speed-ratio.

3.3. Comparison of PIV measurement and CFD simulation

To compare with the results of CFD simulation and PIV experiment, the line data of ensemble averaged velocity fields have been selected from the blade tip vortex core to the boundary. In Fig. 9, the comparison of PIV and CFX with 300rpm and wind velocity is 3.5m/s. It seems that wind velocity of experiment is higher than that in CFD, and at beginning, there is a downward tendency that reflects the situation from upstream to downstream through the core of tip vortex structure. Reading those responses on ensemble averaged velocity field of PIV measurements, it is found that as the relative lower incoming airflow, the tip vortex structures and wake velocity is easier to be influenced because the spiral-shaped blade. And at lower tip-speed-ratio, the influenced region is more widely than higher conditions. At that time, the results of PIV and CFX have a similar trend distribution in Fig. 9. From Fig. 10 and 11, the results are similar with each condition. The flow was mainly attached and only separated at the core of tip vortex. It means that the downstream mean velocity in the core of tip vortex of PIV is lower than that in the CFX simulation. Around the boundary sections of PIV or unsteady state CFX are similar with each other, especially under 500rpm. In case of the incoming wind velocity is 4.5m/s condition, in this case, the PIV result is in good agreement with unsteady state CFX result. By comparison of the ensemble averaged velocity field and pressure field, because the low pressure area of the suction side gradually moved to the blade tip edge, when the dynamic pressure is less than adverse static pressure, the flow cannot stay at the blade any longer, and the boundary layer would separate, then the separated vortex would form. After that the main separated vortex is further increased and the affected region is even larger. The comparison of the PIV measurement with CFD numerical simulation show that the vector diagram nearly agreed with

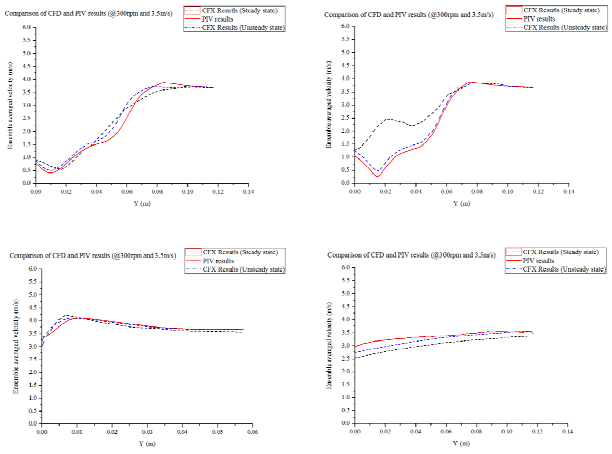

Fig. 9. Comparison of PIV and CFX (steady and unsteady state) results (300rpm and U_∞=3.5m/s)

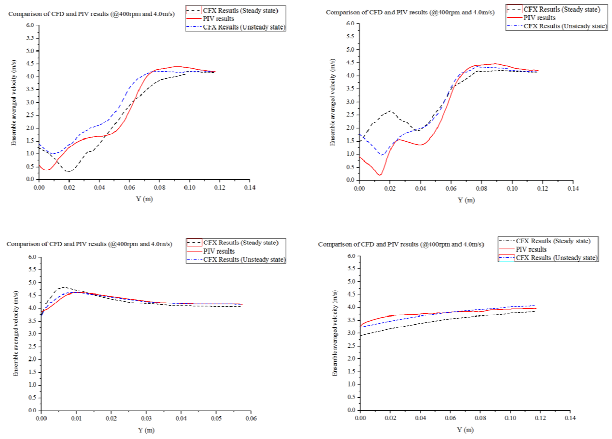

Fig. 10. Comparison of PIV and CFX (steady and unsteady state) results (400rpm and U_∞=4.0m/s)

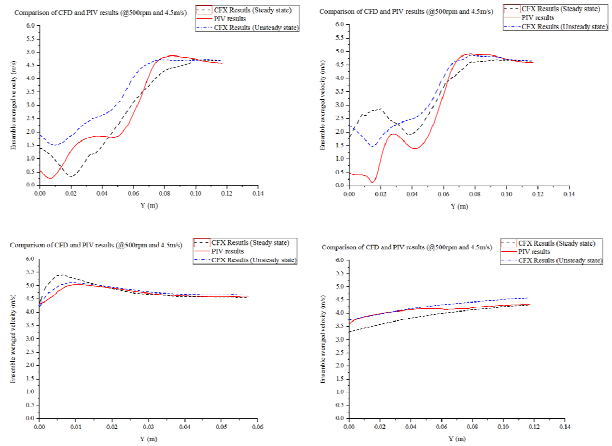

Fig. 11. Comparison of PIV and CFX (steady and unsteady state) results (500rpm and U_∞=4.5m/s)

each other, especially in the shape and the vector trend, as well as the position and size of the tip vortex.

Generally, the flow is explained three governing equation: continuity, momentum, energy. In the case of unsteady state analysis, continuity equation and energy equation are same equations of steady state flow. But unsteady term is consisted of viscous and inertial term.

Momentum equation is normalized by characteristic length, characteristic velocity, and characteristic time. In unsteady state, when the air flow passes the blade, the flow has to accelerate to pass the blade surface. As the air continuous passes the wind turbine blade, it will create a low-pressure area on the tip of the blade because the wind across this area will have higher velocity. But the steady state cases have differences from unsteady state that is due to the fact that steady state simulation does not change the relative position between the blade and incoming airflow. And for the region behind blade, due to the fact that Multiple Reference Frames techniques still employs certain steady state assumption to speed up the calculation and thus the initial relative position will still have influence on the following iterations.

4. Conclusions

In this research, the PIV technique is used for velocity exploration in the near wake of the Archimedes spiral wind turbine blade. Both steady and unsteady simulations of CFD were carried out at the same conditions of experiments. The aerodynamic analysis was carried out after measurements made it possible to obtain the velocity field in the complete plane. Through analysis and comparison, the following conclusions are obtained:

1) When there is no drag torque, the pure blade's rotating speed is influenced by inlet velocity, and the predicted blade's rotating speed approach 500rpm while the inlet velocity is 4.5m/s.

2) The inner low speed section rotated the same turning direction of the blade. The relative velocity of the flow is closed zero to the blade.

3) The analysis of the obtained results shows the interaction between the mean flow at the rotor downstream and the induced velocity due to the tip vortices.

4) Measurements revealed the presence of important vortex structures downstream the hub and near the root of the blade. Some instability of the helical tip vortices is also noted. Because of these fluctuations, the instantaneous velocity field is very rich with information.

5) Due to the PIV experiment, the preferable information of the blade flow under different wind velocity of attack is obtained, which would be very helpful to improve the performance and the design method of Archimedes spiral wind turbine.

6) Unsteady CFD simulation results agree well with those of PIV experiments than the steady state simulation.

Acknowledgements

This study was supported by Human Resources Development Program (No. 20114010203080) and New & Renewable Energy Program (No. 20113030020010) of Korea Institute of Energy Technology Evaluation and Planning (KETEP).

References

[1] World Wind Energy Association. "*Small Wind World Report Summary 2012*". (2012)

[2] Renewable Energy Policy Network for the 21st Century. "*Renewables 2011 Global Status Report*". (2011)

[3] P. J. Kantert. "*Manual for Archimedean Screw Pump*". Hirthammer Verlag, ISBN 978-3-88721-896-6. (2008)

[4] J. J. O'Connor and E. F. Robertson. "*Archimedes of Syracuse*". University of St Andrews. Retrieved 2007-01-02. (2007)

[5] W.A. Timmer and S. Toet. "Verslag van de metingen aan de archimedes in de lage-snelheids windtunnel van dnw". TU Delft. (2009)

[6] Q. Lu, Q. Li, Y.K. Kim and K.C. Kim. "A study on design and aerodynamic characteristics of a spiral-type wind turbine blade". Journal of KSV, Vol. 10, No. 1, pp. 27-33. (2012)

[7] H. Cao. "Aerodynamics Analysis of Small Horizontal Axis Wind Turbine Blades by Using 2D and 3D CFD Modeling". Dissertation of Master degree, University of the Central Lancashire. (2011)

[8] H. Hu, Z. F. Yang and P. Sarkar. "Dynamic wind loads and wake characteristics of a wind turbine model in an atmospheric boundary layer wind". Exp Fluid, DOI 10.1007/s00348-011-1253-5, pp. 1277-1294. (2012)

[9] W. Zhang, C. D. Markfort and F. P. Agel. "Near-wake flow structure downwind of a wind turbine in a turbulent boundary layer". Exp Fluid, DOI 10.1007/s00348-011-1250-8, pp. 1219-1235. (2012)